IEEE Photonics Journal
An IEEE Photonics Society Publication

Open Access

Enhanced Multiple Pulse Position Modulation Aided Reverse Polarity Optical OFDM System With Extended Dimming Control

Volume 10, Number 4, August 2018

Zixian Yang, ***Student Member, IEEE***
Ming Jiang, ***Senior Member, IEEE***
Lin Zhang, ***Member, IEEE***
Hong-Zhou Tan, ***Senior Member, IEEE***

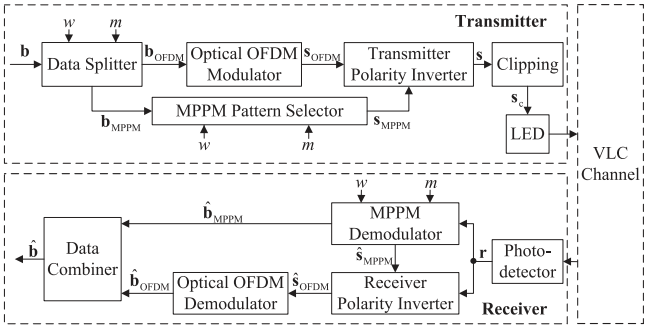

DOI: 10.1109/JPHOT.2018.2838562
1943-0655

Enhanced Multiple Pulse Position Modulation Aided Reverse Polarity Optical OFDM System With Extended Dimming Control

Zixian Yang,[1] ***Student Member, IEEE***,
Ming Jiang,[1,2] ***Senior Member, IEEE***, **Lin Zhang**,[1] ***Member, IEEE***,
and Hong-Zhou Tan,[1,2] ***Senior Member, IEEE***

[1]Sun Yat-sen University, Guangzhou 510275, China
[2]SYSU Shunde Research Institute, Shunde 528300, China

DOI:10.1109/JPHOT.2018.2838562

Manuscript received April 7, 2018; revised May 9, 2018; accepted May 16, 2018. Date of publication May 21, 2018; date of current version June 8, 2018. This work was supported in part by the General Project of National Natural Science Foundation of China under Grants 61771499 and 61473322 and in part by the Basic Research Project of Guangdong Provincial NSF under Grant 2016A030308008.
Corresponding author: Ming Jiang (e-mail: jiangm7@mail.sysu.edu.cn).

Abstract: In this paper, we propose a multiple pulse position modulation (MPPM) aided reverse polarity optical orthogonal frequency division multiplexing scheme that aims to enhance the spectral efficiency (SE) for dimmable visible light communication (VLC) systems. In this scheme, we exploit the MPPM patterns to transmit the extra information bits without the increase of the signal bandwidth and, thus, improving the SE. Specifically, for each frame, the binary information stream is divided into two parallel groups, where the first group is used to select the patterns of MPPM symbols, while the other is modulated by optical OFDM. Then, the time-domain OFDM signal is accommodated by both the "on" and "off" slots of MPPM symbols for transmissions over the VLC channel. With the aid of a forward error correction aided decision feedback approach, the system performance can be further improved. Theoretical analyses on the dimming level, the average power consumption and the frame error probability are provided and verified by simulation results. It is shown that the proposed system with extended dimming control can achieve the highest effective spectral efficiency in most scenarios without substantially increasing the computational complexity, while still maintaining a power consumption level similar to those of the reference systems.

Index Terms: Dimming control, effective spectral efficiency (ESE), multiple pulse position modulation (MPPM), reverse polarity optical orthogonal frequency division multiplexing (RPO-OFDM), visible light communication (VLC)

1. Introduction

With the rapid development and deployment of wireless networks, the spectrum shortage problem concerning conventional radio frequency (RF) systems becomes increasingly severe. Such a problem, however, may be alleviated by employing visible light communication (VLC) technologies, which utilise the visible light spectrum with tera-Hz unregulated bandwidth. Equipped with the light-emitting diodes (LED) that are widely used for illumination [1], VLC systems have the distinct

advantages [2], such as unlicensed spectrum, exemption from interference with RF systems, no electromagnetic radiation, etc.

As a mature technology for RF-based long-term evolution (LTE) systems, orthogonal frequency division multiplexing (OFDM) has also been considered for employment in VLC systems for data rate improvements and inter-symbol-interference (ISI) mitigation. A few optical OFDM methods have been proposed, which can generate real-valued non-negative signals for supporting the intensity modulation and direct detection (IM/DD) functions required in VLC systems, including for example pulse-amplitude-modulated discrete multitone (PAM-DMT) [3], direct current biased optical OFDM (DCO-OFDM), asymmetrically clipped optical OFDM (ACO-OFDM) [4], [5], asymmetrically clipped DC biased optical OFDM (ADO-OFDM) [6], unipolar OFDM (U-OFDM) [7], polar-OFDM (P-OFDM) [8], enhanced U-OFDM (eU-OFDM) [9] and so on. On the other hand, one key advantage offered by VLC is that illumination and data communication services can be simultaneous achieved through specifically designed dimming control functionalities. Typically, digital dimming techniques are preferred [2], since they not only result in less chromaticity shifts in comparison to analog dimming, but also exhibit notable implementational benefits in brightness adjustment with the aid of simple duty cycle adaptation.

Hence, combining OFDM with dimming control schemes has become one of the design targets for pragmatic VLC systems [10]–[13]. For example, the 'on' period of a pulse width modulation (PWM) symbol [10] or a multiple pulse position modulation (MPPM) symbol [11] can be utilised to transmit an OFDM signal. However, both the PWM-OFDM and the MPPM-OFDM schemes mentioned above can lead to a limited data rate, especially when the duty cycle is reduced for lower brightness requirement.

To relax such constraints, the reverse polarity optical OFDM (RPO-OFDM) [12] has been proposed to transmit the signal during both the 'on' and the 'off' durations within one PWM period and to utilise the LED dynamic range while minimising the nonlinear distortion of OFDM signals. Furthermore, asymmetrical hybrid optical OFDM (AHO-OFDM) [13], which combines ACO-OFDM with PAM-DMT, was claimed to achieve good spectral efficiency (SE) with a wide dimming range, though at the cost of high implementational complexity due to the introduction of additional receiver modules as well as an adaptive transmission mechanism.

Against this background, in this paper a new scheme referred to as MPPM-aided RPO-OFDM (MPPM-RPO-OFDM) is proposed. More specifically, the binary information bit stream is divided into two parts, where the first part is used to select the patterns of MPPM symbols based on the MPPM duty cycle and the number of slots in one MPPM symbol, while the second part is modulated by an optical OFDM scheme into both the 'on' and 'off' slots of MPPM symbols using a polarity inverter. Our main contributions include:

- A hybrid structure efficiently amalgamating MPPM and RPO-OFDM technologies is designed for VLC systems with the support of flexible dimming control. By exploiting the MPPM patterns, additional information bits can be transmitted without increasing the system bandwidth, thus achieving a higher SE compared to RPO-OFDM.
- A forward error correction (FEC) aided decision-feedback (DF) approach is proposed, which further improves the link robustness of the hybrid MPPM-RPO-OFDM system.
- The theoretical performance analyses of the proposed system on the dimming level, the average power consumption and the frame error probability (FEP) are provided, taking into account signal distortions caused by clipping and MPPM demodulation errors in practical VLC systems.
- Extensive simulation results are offered, which validate our theoretical derivations and demonstrate that our method outperforms a few existing schemes such as MPPM-OFDM, RPO-OFDM and AHO-OFDM in terms of effective spectral efficiency (ESE). Furthermore, such benefits are achievable without largely increasing the computational complexity, while still maintaining similar power consumption.

The remaining part of this paper is organised as follows. The details of the proposed MPPM-RPO-OFDM system including the corresponding theoretical analysis are presented in Section 2, followed by the design of the enhanced MPPM-RPO-OFDM scheme in Section 3. Simulation results are provided in Section 4. Finally, Section 5 concludes our findings.

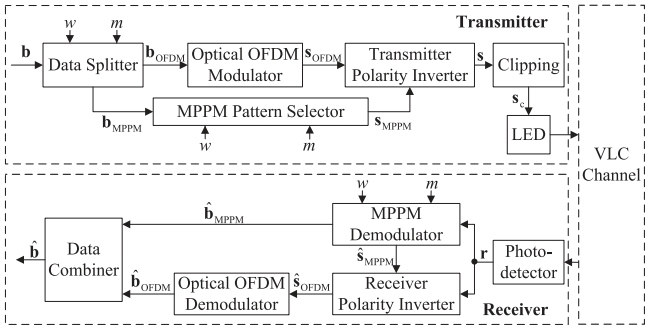

Fig. 1. The schematic of the proposed MPPM-RPO-OFDM system.

2. The Proposed MPPM-RPO-OFDM System

2.1 System Model

The schematic of the proposed MPPM-RPO-OFDM system is shown in Fig. 1. At the transmitter side, the data splitter divides the input binary information sequence $\mathbf{b}$ into two parallel streams, where the first one $\mathbf{b}_{\text{MPPM}}$ is used for MPPM pattern selection, and the other one $\mathbf{b}_{\text{OFDM}}$ is subjected to optical OFDM modulation. Then, the OFDM signal $\mathbf{s}_{\text{OFDM}}$ is further modulated into the MPPM symbols $\mathbf{s}_{\text{MPPM}}$ with the aid of the transmitter polarity inverter (TPI), whose output signal $\mathbf{s}$ is clipped to $\mathbf{s}_{\text{c}}$ for transmission through an LED.

At the receiver, the optical signal is first detected by the photo-detector (PD), followed by the MPPM demodulation process. The demodulated MPPM symbols $\hat{\mathbf{s}}_{\text{MPPM}}$ can therefore be utilised by the receiver polarity inverter (RPI) to recover the estimate of the transmitted OFDM signal, denoted by $\hat{\mathbf{s}}_{\text{OFDM}}$. Finally, the bits respectively recovered by the optical OFDM demodulator $\hat{\mathbf{b}}_{\text{OFDM}}$ and the MPPM demodulator $\hat{\mathbf{b}}_{\text{MPPM}}$ are combined to form the estimated information bit sequence $\hat{\mathbf{b}}$.

2.1.1 Transmitter

a) Data Splitting: The data splitter divides $\mathbf{b}$ into two streams of $\mathbf{b}_{\text{MPPM}}$ and $\mathbf{b}_{\text{OFDM}}$ on a frame-by-frame manner, where each frame has the same length of T_{F}. For each frame, the first bit stream $\mathbf{b}_{\text{MPPM}}$ is embedded into the MPPM symbols. Specifically, for each (m, w)-MPPM symbol there exist $C_m^w = \frac{m!}{w!(m-w)!}$ possible patterns, where C denotes the combination operator, m is the number of slots in each MPPM symbol, and $w \in \{0, 1, \ldots, m\}$ with $d = \frac{w}{m}$ representing the duty cycle of MPPM symbols. Thus, one MPPM symbol accommodates a number of $\mathcal{B}_{\text{MPPM}} = \lfloor \log_2(C_m^w) \rfloor$ bits, where $\lfloor x \rfloor$ indicates the maximum integer less than or equal to x.

On the other hand, the second bit steam output by the bit splitter $\mathbf{b}_{\text{OFDM}}$ is forwarded to the optical OFDM modulator, where any optical OFDM scheme, such as DCO-OFDM [5], ACO-OFDM [5], ADO-OFDM [6], U-OFDM [7], P-OFDM [8], eU-OFDM [9], etc., may theoretically be employed. Note however that if DCO-OFDM or ADO-OFDM is used, the DC bias should not be too large, otherwise the difference between the average optical powers of the OFDM signals camped on the 'on' and the 'off' levels may be too small, thus reducing the effectiveness of the proposed dimming control mechanism based on MPPM patterns. Hence, the optical OFDM schemes without DC bias are more suitable for employment in the proposed scheme. In the sequel, ACO-OFDM is used as the main example to show our design concept, though other schemes, for instance eU-OFDM, can also be applicable.

In the example system, one OFDM symbol accommodates $\mathcal{B}_{\text{OFDM}} = \frac{N}{4} \log_2 M$ bits, where N is the number of subcarriers and M is the number of signal points of the constellation employed, for example quadrature amplitude modulation (QAM). Each data frame in the proposed hybrid system contains a total of l MPPM symbols and p OFDM symbols, where we have $l, p \in \mathbb{Z}^+$. Fig. 2 shows an example configuration of $p = 2$ and $l = 5$.

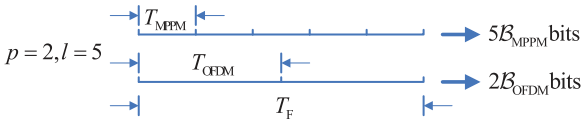

Fig. 2. An example of the frame structure.

TABLE 1
An Example of MPPM Mapping Rules

Bits	{00}	{01}	{10}	{11}
Indices of 'on' slots	{1, 2}	{1, 3}	{1, 4}	{2, 3}

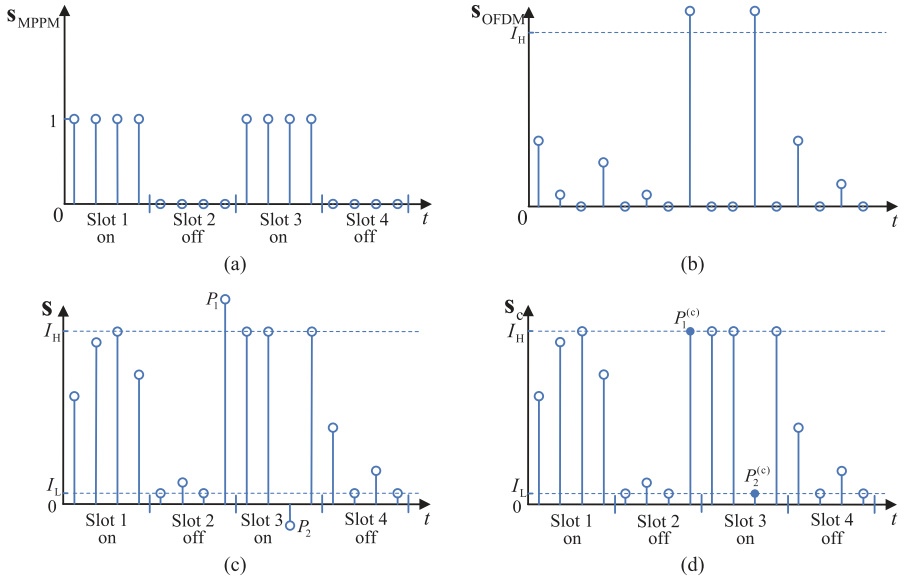

Fig. 3. An example of the modulation process. (a) MPPM pattern selection. (b) The ACO-OFDM signal. (c) The hybrid signal of (3). (d) The clipped transmit signal.

As a result, the number of bits transmitted within one data frame, denoted by $\mathcal{B}_{\text{F}}$, is equal to

$$\mathcal{B}_{\text{F}} = l \cdot \mathcal{B}_{\text{MPPM}} + p \cdot \mathcal{B}_{\text{OFDM}} = l \left\lfloor \log_2(C_m^w) \right\rfloor + \frac{pN}{4} \cdot \log_2 M. \tag{1}$$

Obviously, the proposed hybrid design accommodates more bits than MPPM or ACO-OFDM alone. Accordingly, the frame length T_{F} can be formulated as

$$T_{\text{F}} = l \cdot T_{\text{MPPM}} = p \cdot T_{\text{OFDM}}, \tag{2}$$

where $T_{\text{MPPM}} = a \cdot m \cdot T_{\text{s}}$ and T_{OFDM} denote the periods of MPPM and cyclic-prefix-excluded ACO-OFDM symbols, respectively, while a denotes the number of samples in each MPPM slot and $T_{\text{s}} = \frac{T_{\text{OFDM}}}{N}$ refers to the sampling interval. Therefore, we have $l \cdot a \cdot m = p \cdot N$ and the data rate of the proposed system is $R_{\text{b}} = \frac{\mathcal{B}_{\text{F}}}{T_{\text{F}}}$.

b) MPPM Pattern Selection: The MPPM patterns may be selected according to simple mapping rules shown in Table 1. For example, for a (4, 2) MPPM symbol, there are $C_4^2 = 6$ possible patterns, from which 4 patterns can be selected to represent $\mathcal{B}_{\text{MPPM}} = 2$ bits. In each selected pattern, two slots are labelled as 'on' and the remaining as 'off'. Assuming $a = 4$, Fig. 3(a) shows an example of modulating the bit pair of '01' to form the MPPM signal $\mathbf{s}_{\text{MPPM}}$, which is also illustrated in Fig. 1, with values 1 and 0 at its 'on' and 'off' slots, respectively.

c) Polarity Inversion and Clipping: As illustrated in Fig. 1, after the MPPM pattern selection and ACO-OFDM modulation procedures, the OFDM signal $\mathbf{s}_{\text{OFDM}}$ is further modulated into both 'on'

and 'off' slots of the MPPM symbols $\mathbf{s}_{\text{MPPM}}$ with the aid of the TPI, as follows

$$s_k = \begin{cases} I_{\text{H}} - s_{\text{OFDM},k}, & s_{\text{MPPM},k} = 1 \\ I_{\text{L}} + s_{\text{OFDM},k}, & s_{\text{MPPM},k} = 0 \end{cases}, k = 1, \ldots, \mathcal{K}, \tag{3}$$

where $\mathcal{K} = l \cdot m \cdot a$, while I_{H} and I_{L} are the rated maximum and minimum current levels of the LED linear dynamic range [12] respectively. The variables s_k, $s_{\text{OFDM},k}$ and $s_{\text{MPPM},k}$ in (3) denote the kth element of $\mathbf{s}$, $\mathbf{s}_{\text{OFDM}}$ and $\mathbf{s}_{\text{MPPM}}$, respectively. The electrical signal power of $\mathbf{s}_{\text{OFDM}}$ is denoted as $P_{\text{OFDM}} = \frac{\sigma^2}{2}$, where σ is the standard deviation of the corresponding bipolar OFDM signal. Fig. 3(b) and (c) provide examples of $\mathbf{s}_{\text{OFDM}}$ and $\mathbf{s}$, respectively. Then, the clipping operation will be performed on $\mathbf{s}$ to ensure that it falls within the range of $[I_{\text{L}}, I_{\text{H}}]$, resulting in

$$s_{\text{c},k} = \begin{cases} I_{\text{L}}, & s_k \leq I_{\text{L}} \\ s_k, & I_{\text{L}} < s_k < I_{\text{H}} \\ I_{\text{H}}, & s_k \geq I_{\text{H}} \end{cases}, k = 1, \ldots, \mathcal{K}, \tag{4}$$

where $s_{\text{c},k}$ is the kth sample of the clipped signal $\mathbf{s}_{\text{c}}$ exemplified in Fig. 3(d), which will be transmitted through an indoor VLC channel.

2.1.2 Receiver

At the receiver, based on frame-by-frame demodulation under a sampling period of T_{s}, the PD's output signal is

$$\mathbf{r} = \mathbf{s}_{\text{c}} + \mathbf{n}, \tag{5}$$

where $\mathbf{n}$ is the additive white Gaussian noise (AWGN) with variance of σ_{n}^2. Note that the knowledge of the quantised duty cycle d may be transmitted through dedicated control channels and is therefore assumed to be known at the receiver. In the special case of $d = 0$ or $d = 1$, it is easy to obtain $\hat{\mathbf{s}}_{\text{OFDM}}$ directly. In other cases, similar to [11], the MPPM demodulation process should first be invoked before OFDM demodulation. The average sample value at the vth slot of the uth MPPM symbol, denoted as $\bar{r}_{u,v}$, can be calculated by

$$\bar{r}_{u,v} = \frac{1}{a} \cdot \sum_{k=(u-1)ma+(v-1)a+1}^{(u-1)ma+va} r_k, \; u = 1, \ldots, l; \; v = 1, \ldots, m, \tag{6}$$

where r_k denotes the kth element of $\mathbf{r}$. Next, a total of w largest values are selected from the set $\{\bar{r}_{u,v} | v = 1, \ldots, m\}$, which will be considered as the 'on' slots of the uth MPPM symbol, while the remaining slots are assumed to be the 'off' slots. Then, we may demodulate the MPPM symbol with the aid of Table 1 before $\hat{\mathbf{s}}_{\text{MPPM}}$ and $\hat{\mathbf{b}}_{\text{MPPM}}$ are obtained. Subsequently, based on $\hat{\mathbf{s}}_{\text{MPPM}}$, the RPI function in Fig. 1 is invoked to produce the estimated ACO-OFDM signal as

$$\hat{s}_{\text{OFDM},k} = \begin{cases} I_{\text{H}} - r_k, & \hat{s}_{\text{MPPM},k} = 1 \\ r_k - I_{\text{L}}, & \hat{s}_{\text{MPPM},k} = 0 \end{cases}, k = 1, \ldots, \mathcal{K}, \tag{7}$$

where $\hat{s}_{\text{OFDM},k}$ and $\hat{s}_{\text{MPPM},k}$ denote the kth element of $\hat{\mathbf{s}}_{\text{OFDM}}$ and $\hat{\mathbf{s}}_{\text{MPPM}}$ respectively. Then $\hat{\mathbf{s}}_{\text{OFDM}}$ is subject to OFDM demodulation for obtaining $\hat{\mathbf{b}}_{\text{OFDM}}$ seen in Fig. 1. Finally, $\hat{\mathbf{b}}_{\text{MPPM}}$ and $\hat{\mathbf{b}}_{\text{OFDM}}$ are combined to form the estimated bit stream $\hat{\mathbf{b}}$.

2.2 Theoretical Performance Analysis

In this section, we analyse the theoretical performance of the proposed MPPM-RPO-OFDM system from the aspects of dimming level, average electrical LED power consumption and FEP, respectively. Relevant theoretical derivations are also provided for some reference systems, for example RPO-OFDM and MPPM-OFDM, to facilitate the performance analysis and comparison in Section 4.

2.2.1 Dimming Level

The dimming level is defined as [13]

$$\eta = \frac{\bar{I} - I_{\mathrm{L}}}{I_{\mathrm{H}} - I_{\mathrm{L}}}, \tag{8}$$

where $\bar{I}$ is the average LED current. The values of $\bar{I}$ for MPPM-RPO-OFDM, RPO-OFDM and MPPM-OFDM systems, denoted as $\bar{I}_{\mathrm{MRO}}$, $\bar{I}_{\mathrm{RO}}$ and $\bar{I}_{\mathrm{MO}}$, respectively, can be calculated as follows.

Firstly, the value of $\bar{I}_{\mathrm{MRO}}$ may be formulated as

$$\bar{I}_{\mathrm{MRO}} = \left(I_{\mathrm{L}} + \bar{I}_{\mathrm{OFDMc}}\right)(1-d) + \left(I_{\mathrm{H}} - \bar{I}_{\mathrm{OFDMc}}\right)d, \tag{9}$$

where $\bar{I}_{\mathrm{OFDMc}}$ is the average current, which corresponds to the signal after clipping $\mathbf{s}_{\mathrm{OFDM}}$ for fitting the range of $[0, I_{\mathrm{H}} - I_{\mathrm{L}}]$. According to [14], we may obtain $\bar{I}_{\mathrm{OFDMc}}$ by

$$\bar{I}_{\mathrm{OFDMc}} = Q\left(\tfrac{I_{\mathrm{H}}-I_{\mathrm{L}}}{\sigma}\right)\cdot(I_{\mathrm{H}} - I_{\mathrm{L}}) - \phi\left(\tfrac{I_{\mathrm{H}}-I_{\mathrm{L}}}{\sigma}\right)\cdot\sigma + \tfrac{\sigma}{\sqrt{2\pi}}, \tag{10}$$

where $\sigma = \sqrt{2P_{\mathrm{OFDM}}}$, while $Q(\cdot)$ is the Q-function given by $Q(x) = \frac{1}{\sqrt{2\pi}}\cdot\int_x^{\infty}\exp\left(-\frac{t^2}{2}\right)\mathrm{d}t$ and $\phi(x) = \frac{1}{\sqrt{2\pi}}\cdot\exp\left(-\frac{x^2}{2}\right)$.

Since the distribution of the amplitude of a RPO-OFDM signal is the same as that of MPPM-RPO-OFDM, (9) can also be used to calculate $\bar{I}_{\mathrm{RO}}$ for the reference RPO-OFDM system, namely $\bar{I}_{\mathrm{RO}} = \bar{I}_{\mathrm{MRO}}$. Furthermore, in the reference MPPM-OFDM system assuming ACO-OFDM, we have

$$\bar{I}_{\mathrm{MO}} = \left(I_{\mathrm{L}} + \bar{I}_{\mathrm{OFDMc}}\right)d. \tag{11}$$

With the aid of (8)–(11), we note that η is a linear function of d and depends on P_{OFDM} in all the three systems. By adjusting d from 0 to 1, η would change linearly within a range determined by P_{OFDM}. Therefore, we propose that dimming is controlled in a way as follows. As the initial step, we dim the LED by adapting $d = \frac{w}{m}$. If η needs to be further reduced (increased) after $d = 0$ ($d = 1$) is reached for implementing an *extended* dimming control, we suggest that I_{L} (I_{H}) is transmitted at the first $\alpha(\alpha = 0, \ldots, m)$ slots and $s_{\mathrm{c},k}$ at the remaining $m - \alpha$ slots, of the MPPM symbol concerned. Through this way, η can be extended to both ends of 0% and 100% at the cost of a compromised achievable data rate.

2.2.2 Average Electrical LED Power Consumption

We define the average electrical LED power $\bar{P}_{\mathrm{LED}}$ for MPPM-RPO-OFDM, RPO-OFDM and MPPM-OFDM systems as $\bar{P}_{\mathrm{LED,MRO}}$, $\bar{P}_{\mathrm{LED,RO}}$ and $\bar{P}_{\mathrm{LED,MO}}$, respectively. Then, for MPPM-RPO-OFDM we may calculate

$$\bar{P}_{\mathrm{LED,MRO}} = \phi\left(\frac{I_{\mathrm{H}} - I_{\mathrm{L}}}{\sigma}\right)\left[\sigma(2d-1)(I_{\mathrm{H}} + I_{\mathrm{L}})\right] + \left[\frac{1}{2} - Q\left(\frac{I_{\mathrm{H}} - I_{\mathrm{L}}}{\sigma}\right)\right]\left[(2d-1)I_{\mathrm{H}}^2 + (1-d)I_{\mathrm{L}}^2 + \sigma^2\right] + \frac{I_{\mathrm{H}}^2}{2} + \frac{2\sigma I_{\mathrm{L}}(1-d) - 2\sigma I_{\mathrm{H}}d}{\sqrt{2\pi}}. \tag{12}$$

For the same reason pointed out in Section 2.2.1 with respect to $\bar{I}_{\mathrm{RO}}$, (12) can also be used to calculate $\bar{P}_{\mathrm{LED,RO}}$, namely $\bar{P}_{\mathrm{LED,RO}} = \bar{P}_{\mathrm{LED,MRO}}$.

Moreover, for MPPM-OFDM system, we have

$$\bar{P}_{\mathrm{LED,MO}} = Q\left(\frac{I_{\mathrm{H}} - I_{\mathrm{L}}}{\sigma}\right)\cdot\left(I_{\mathrm{H}}^2 - \sigma^2 - I_{\mathrm{L}}^2\right)d - \phi\left(\frac{I_{\mathrm{H}} - I_{\mathrm{L}}}{\sigma}\right)\cdot\sigma(I_{\mathrm{H}} + I_{\mathrm{L}})d + \frac{\sigma^2 d + 2I_{\mathrm{L}}^2 d}{2} + \frac{2I_{\mathrm{L}}\sigma d}{\sqrt{2\pi}}. \tag{13}$$

With the aid of (12) and (13), which are derived in Appendix A, it can be seen that $\bar{P}_{\mathrm{LED}}$ is a linear function of d in all the three systems. Similar to the range of η, the range of $\bar{P}_{\mathrm{LED}}$ is also determined by P_{OFDM}.

2.2.3 Frame Error Probability

In an OFDM system employing a large number of subcarriers, the time-domain OFDM signal samples may be assumed to be mutually independent and to follow Gaussian distribution [15]. Therefore, the probabilities of correct demodulation of the MPPM symbol and the OFDM symbol, denoted as $\rho_{\mathrm{MPPM}}^{(\mathrm{c})}$ and $\rho_{\mathrm{OFDM}}^{(\mathrm{c})}$, respectively, may be considered as time-invariable. If perfect synchronisation is assumed, the FEP of MPPM-RPO-OFDM can be calculated by

$$\rho_{\mathrm{F}}^{(\mathrm{e})} = 1 - \left[\rho_{\mathrm{MPPM}}^{(\mathrm{c})}\right]^{l} \cdot \left[\rho_{\mathrm{OFDM}}^{(\mathrm{c})}\right]^{p}, \tag{14}$$

and $\rho_{\mathrm{OFDM}}^{(\mathrm{c})}$ is formulated as

$$\rho_{\mathrm{OFDM}}^{(\mathrm{c})} = \left[1 - \rho_{\mathrm{QAM}}^{(\mathrm{e})}\right]^{\frac{N}{4}}, \tag{15}$$

where the M-QAM symbol error probability (SEP) in ACO-OFDM systems, $\rho_{\mathrm{QAM}}^{(\mathrm{e})}$, is specified by [16]

$$\rho_{\mathrm{QAM}}^{(\mathrm{e})} = 4\left(\frac{\sqrt{M}-1}{\sqrt{M}}\right) Q\left(\sqrt{\frac{3E_{\mathrm{s}}}{N_0(M-1)}}\right) - 4\left(\frac{\sqrt{M}-1}{\sqrt{M}}\right)^2 \left[Q\left(\sqrt{\frac{3E_{\mathrm{s}}}{N_0(M-1)}}\right)\right]^2. \tag{16}$$

In order to calculate $\rho_{\mathrm{QAM}}^{(\mathrm{e})}$ of (16), the signal-to-noise ratio (SNR) per QAM symbol for the clipped ACO-OFDM signal, $\frac{E_{\mathrm{s}}}{N_0}$, has to be obtained. More specifically, with the aid of [14, (15) (16)], we have

$$\frac{E_{\mathrm{s}}}{N_0} = \frac{K^2 \cdot 2\sigma^2}{\sigma_{\mathrm{cl}}^2 + \sigma_{\mathrm{n}}^2}, \tag{17}$$

where the attenuation factor K and the variance of the clipping noise σ_{cl}^2 are specified by $K = \frac{1}{2} - Q\left(\frac{l_{\mathrm{H}}-l_{\mathrm{L}}}{\sigma}\right)$ and $\sigma_{\mathrm{cl}}^2 = \sigma^2\left[K - 2K^2 - \phi\left(\frac{l_{\mathrm{H}}-l_{\mathrm{L}}}{\sigma}\right)\cdot\left(\frac{l_{\mathrm{H}}-l_{\mathrm{L}}}{\sigma}\right) + Q\left(\frac{l_{\mathrm{H}}-l_{\mathrm{L}}}{\sigma}\right)\cdot\left(\frac{l_{\mathrm{H}}-l_{\mathrm{L}}}{\sigma}\right)^2\right]$ [14], respectively. On the other hand, based on the derivations in Appendix B, we have

$$\rho_{\mathrm{MPPM}}^{(\mathrm{c})} = w\int_{-\infty}^{+\infty} f_{\bar{r}_{\mathrm{off}}}(x)\left[\int_{-\infty}^{x} f_{\bar{r}_{\mathrm{off}}}(t)\mathrm{d}t\right]^{w-1} \cdot \left[\int_{-\infty}^{l_{\mathrm{H}}+l_{\mathrm{L}}-x} f_{\bar{r}_{\mathrm{off}}}(t)\mathrm{d}t\right]^{m-w} \mathrm{d}x, \tag{18}$$

where $w = md \in \{0, 1, \ldots, m\}$, while

$$f_{\bar{r}_{\mathrm{off}}}(x) = \frac{1}{\sqrt{2\pi}}\int_{-\infty}^{+\infty} \phi\left(\frac{\sigma_{\mathrm{n}}\omega}{\sqrt{a}}\right)\left[\varphi_{s_{\mathrm{c,off}}}\left(\frac{\omega}{a}\right)\right]^a \exp\left(-\mathrm{j}\omega x\right)\mathrm{d}\omega \tag{19}$$

is the probability density function (PDF) of $\bar{r}_{u,v}$ defined in (6), where the subscript 'off' in $f_{\bar{r}_{\mathrm{off}}}(x)$ indicates the 'off' slots of an MPPM symbol and $\mathrm{j} = \sqrt{-1}$. Note that $\varphi_{s_{\mathrm{c,off}}}(\omega)$ in (19) represents the characteristic function (CF) of $\mathbf{s}_{\mathrm{c}}$ at the 'off' slots, which can be obtained by integrating the product of its corresponding PDF $f_{s_{\mathrm{c,off}}}(x)$ and $\exp(\mathrm{j}\omega x)$ [17] as follows

$$\begin{aligned}\varphi_{s_{\mathrm{c,off}}}(\omega) &= \int_{-\infty}^{+\infty} f_{s_{\mathrm{c,off}}}(x)\exp\left(\mathrm{j}\omega x\right)\mathrm{d}x \\ &= \frac{1}{2}\exp\left(\mathrm{j}\omega l_{\mathrm{L}}\right) + Q\left(\frac{l_{\mathrm{H}}-l_{\mathrm{L}}}{\sigma}\right)\exp\left(\mathrm{j}\omega l_{\mathrm{H}}\right) + \int_{l_{\mathrm{L}}}^{l_{\mathrm{H}}} \frac{1}{\sigma}\phi\left(\frac{x-l_{\mathrm{L}}}{\sigma}\right)\exp\left(\mathrm{j}\omega x\right)\mathrm{d}x,\end{aligned} \tag{20}$$

where $f_{s_{\mathrm{c,off}}}(x)$ is given by (22) in Appendix A.

By substituting (15) and (18) into (14), the theoretical FEP of the proposed MPPM-RPO-OFDM system can be obtained. However, note that (18) involves multiple infinite integrals and is difficult to be solved theoretically. Thus, we propose to solve it numerically. Specifically, we evaluate the integrals using high-order global adaptive Gauss-Kronrod quadrature and apply an approximation of (18), which is developed in Appendix C for improving the computational efficiency.

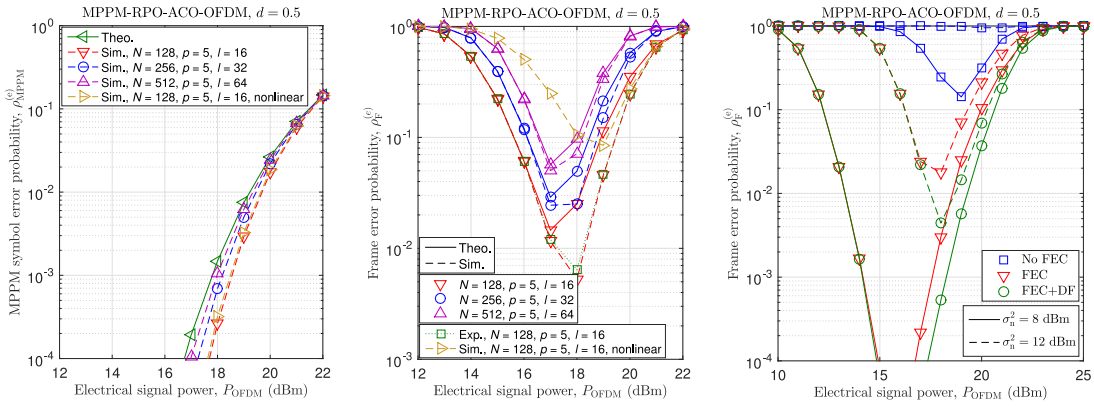

Fig. 4. The MPPM-related SEP and the overall FEP performances of the MPPM-RPO-ACO-OFDM system. (a) MPPM SEP, $\sigma_{\mathrm{n}}^2 = 5\,\mathrm{dBm}$. (b) Overall FEP, $\sigma_{\mathrm{n}}^2 = 5\,\mathrm{dBm}$. (c) Overall FEP, $\sigma_{\mathrm{n}}^2 = \{8, 12\}\,\mathrm{dBm}$.

3. Enhanced MPPM-RPO-OFDM With FEC and DF

The proposed MPPM-RPO-OFDM scheme of Section 2 can be improved by employing FEC and DF approaches. More specifically, at the transmitter side, two channel encoders can be used to protect the information bit streams $\mathbf{b}_{\mathrm{MPPM}}$ and $\mathbf{b}_{\mathrm{OFDM}}$, which are to be delivered by MPPM and OFDM symbols, respectively. The FEC-coded bits will then be subjected to the same procedure as described in Section 2.

At the receiver side, the same demodulation procedures can be invoked first on MPPM and then on OFDM symbols to obtain the estimated coded bit streams, followed by the FEC decoders which would help to improve the error performance of the system. Moreover, the achievable performance can be further enhanced if a DF mechanism is exploited. More explicitly, we can re-encode the FEC-decoded MPPM bits, and use the re-encoded bits to generate the corresponding MPPM symbols, which are expected to be an enhanced version of $\hat{\mathbf{s}}_{\mathrm{MPPM}}$ seen in Fig 1, denoted as $\hat{\mathbf{s}}'_{\mathrm{MPPM}}$ here. Under such a DF mechanism, the demodulation of OFDM bits can be based on $\hat{\mathbf{s}}'_{\mathrm{MPPM}}$, thus resulting in a higher reliability.

4. Simulation Results

In this section, the performance of the proposed MPPM-RPO-OFDM system is evaluated and compared with those of some benchmark schemes, namely the RPO-OFDM [12], MPPM-OFDM [11] and AHO-OFDM [13] systems. The values of the main parameters used are $p = 5$, $l = 16$, $m = 10$, $N = 128$, $a = 4$, $M = 4$, $I_{\mathrm{L}} = 0\,\mathrm{A}$, $I_{\mathrm{H}} = 1\,\mathrm{A}$ unless otherwise specified. Perfect synchronisation and the same system bandwidth of $B = \frac{1}{T_{\mathrm{s}}}$ are assumed in all schemes. A typical indoor VLC channel with only line-of-sight (LOS) propagation is considered.

4.1 Uncoded Results

Fig. 4(a) and (b) show the MPPM-related SEP and the overall FEP performances of the MPPM-RPO-ACO-OFDM system, respectively. Both subfigures assume $d = 0.5$ and $\sigma_{\mathrm{n}}^2 = 5\,\mathrm{dBm}$, where $\rho_{\mathrm{MPPM}}^{(\mathrm{e})} = 1 - \rho_{\mathrm{MPPM}}^{(\mathrm{c})}$, and $\rho_{\mathrm{MPPM}}^{(\mathrm{c})}$ is calculated according to the approximated theoretical model of Appendix C. We can see from Fig. 4(a) and (b) that the simulated and the theoretical results match better as the number of subcarriers N increases. This validates our analysis in Section 2.2 that when N has a small value, for example 128, independent Gaussian approximation does not hold and thus a relative divergence between theoretical and simulated performances is observed.

Moreover, note from Fig. 4(b) that in all cases, the FEP performances of the MPPM-RPO-ACO-OFDM system exhibit a 'V'-shape upon the increase of P_{OFDM}. The phenomenon can be explained as follows. Firstly, the initially increased P_{OFDM} boosts the power of QAM symbols accommodated

by the OFDM symbols, hence helps to reduce FEP. However, further increasing P_{OFDM} leads to not only more clipping noise, but also the cross talks of the average sample values $\bar{r}_{u,v}$ between the 'off' and 'on' slots due to the characteristics of the RPO mechanism. Naturally, this would have a negative impact on the demodulation of MPPM symbols, as verified by Fig. 4(a), and then on the demodulation of OFDM symbols, thus increasing the FEP, as shown in Fig. 4(b).

As a further investigation, we have also obtained the experimental FEP results of the MPPM-RPO-ACO-OFDM system, as indicated by the green dotted line with square markers in Fig. 4(b). In this experiment, NI USRP-2920 was used to pre-process the transmit signal and post-process the received signal with the aid of a computer. The LED transmitter, LED Engin LZC-03MC00, and the PD receiver, HAMAMATSU S6801, were placed on a table in a room with a distance of 80 cm between them. With the aid of an optical lens placed in the middle of the transmitter and the receiver, the received SNR at the PD can be easily tuned to meet the noise variance requirement in the experiment. From Fig. 4(b), we can that the measured results match well with the simulated ones.

Moreover, the achievable performance of the proposed system may be affected by the LED nonlinear transfer characteristics, including for example the nonlinear variation of optical power against the forward current [18] between I_{H} and I_{L}, and the nonlinearity resulting from the voltage-to-current (V/I) conversion at the LED. For the first type of nonlinearity, we simulate the MPPM-related SEP and the overall FEP results based on the quadratic nonlinear blue LED model with $a_0 = -0.3251$, $a_1 = 1.321$, $a_2 = 0.0037$ [18], in Fig. 4(a) and (b), respectively, where a_{i} ($i = 0, 1, 2$) are the quadratic polynomial coefficients. It is shown that this kind of LED nonlinear transfer characteristics affects the overall FEP, though it has little impact on the MPPM-related SEP. Such results are expected, as the OFDM symbols in the proposed hybrid system may be sensitive to the LED nonlinearity due to the potential cross-talks between the subcarriers. However, the MPPM symbols are more robust against the LED nonlinear transfer characteristics, which usually produce only a small variation when compared to the detection threshold of the MPPM signal, which also has a relatively longer symbol duration that potentially offers time diversity. Such a small impact may therefore be well mitigated through some smoothing or averaging operations on the samples at the MPPM slots. On the other hand, to compensate the performance loss of the overall FEP, one viable solution would be to employ some pre-compensation methods, such as those of [18], [19], to produce synthetised linear transfer characteristics between I_{H} and I_{L}. In addition, the second type of nonlinearity mentioned above may also be completely removed with the aid of appropriately designed V/I transducers [20]. Further investigations on the aspect of LED nonlinear transfer characteristics are left to future studies.

4.2 Coded Results

In all the FEC-aided simulations presented in this subsection, we used a convolutional code with a coding rate of $R_{\text{c}} = 0.5$.

4.2.1 Error Performance: Assuming $d = 0.5$, Fig. 4(c) shows the FEP performances of the enhanced MPPM-RPO-ACO-OFDM system equipped with FEC under different noise powers. At the left part of Fig. 4(c), when P_{OFDM} is very low, the system's FEP performance is mainly restricted by poor OFDM demodulation regardless of the employment of DF. In contrast, when P_{OFDM} increases, the achievable FEP performance contributed by improved OFDM demodulation becomes restricted by the reduced MPPM performance, as discussed in Section 4.1. In this case, introducing the DF mechanism can help to enhance the MPPM performance, thus alleviating the error propagation effect due to erroneous MPPM detection results. This beneficial effect then contributes to an improved OFDM demodulation performance. Eventually, it leads to a better overall FEP performance, as shown in the middle-to-right part of Fig. 4(c).

4.2.2 Dimming Level and Electrical LED Power: Fig. 5 illustrates η and $\bar{P}_{\text{LED}}$ as a function of the average electrical ACO-OFDM signal power, P_{OFDM}, assuming fixed $d = 0$ and $d = 1$, respectively. It shows that theoretical and simulation results match well, validating our analyses in Section 2.2.1 and Section 2.2.2.

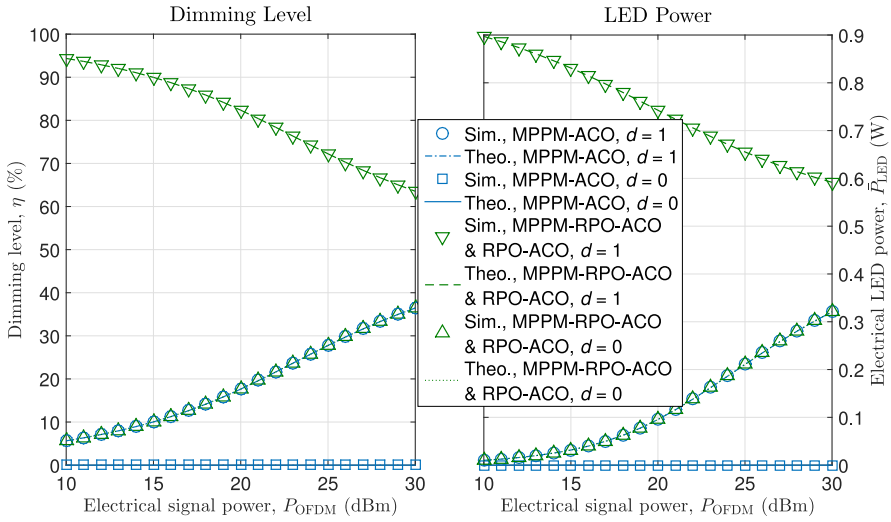

Fig. 5. The dimming level and electrical LED power of MPPM-RPO-ACO-OFDM, MPPM-ACO-OFDM, and RPO-ACO-OFDM systems assuming $d \in \{0, 1\}$.

TABLE 2
An Example Showing the Number of Information Bits Accommodated by MPPM Pattern

Duty cycle, d	OFDM bits	MPPM bits	SE improvement
0, 1	160	0	0%
0.1, 0.9	160	24	15%
0.2, 0.8	160	40	25%
0.3, 0.7	160	48	30%
0.4, 0.5, 0.6	160	56	35%

4.2.3 Effective Spectral Efficiency: One of the advantages offered by the proposed MPPM-RPO-OFDM system is that it can deliver additional bits through the MPPM pattern on top of OFDM modulation. As an example, in Table 2 we outline the number of bits accommodated by the half-rate coded MPPM-RPO-ACO-OFDM system at different duty cycles, assuming 160 information bits are transmitted by OFDM within a frame. In this case, up to 56 additional information bits can be delivered by the MPPM pattern, thus improving the SE by up to 35%.

As a further investigation, we compare the various systems based on the ESE metric, which takes into account the link errors and thus reflects an *error-free* SE [21]. With the employment of FEC codes, ESE can be defined as

$$\gamma = \frac{\left[1 - \rho_{\mathrm{F}}^{(\mathrm{e})}\right] \mathcal{B}_{\mathrm{F}} R_{\mathrm{c}}}{T_{\mathrm{F}} B} = \frac{\left[1 - \rho_{\mathrm{F}}^{(\mathrm{e})}\right] \mathcal{B}_{\mathrm{F}} R_{\mathrm{c}}}{N_{\mathrm{s}} T_{\mathrm{s}} B} = \frac{\left[1 - \rho_{\mathrm{F}}^{(\mathrm{e})}\right] \mathcal{B}_{\mathrm{F}} R_{\mathrm{c}}}{N_{\mathrm{s}}}. \tag{21}$$

For fair comparison, the average values of $\mathcal{B}_{\mathrm{F}}$ in (21) for all systems were set to be equal or similar to 390 coded bits per frame, by adjusting the number of samples per frame, N_{s}. ACO-OFDM and three-layer eU-OFDM [9] were evaluated in all systems, while MPPM-DCO-OFDM [11] was also included as reference. For each individual scheme, preliminary tests were conducted on the corresponding parameters, such as P_{OFDM} and a, to find out a configuration that yields the best γ for that scheme. Then, using a half-rate convolutional code and the proposed DF approach of Section 3, in Fig. 6(a) we compare γ of all systems as a function of η under their respective best configurations, assuming $\sigma_{\mathrm{n}}^2 = 8$ dBm. Note that the dimming control strategy proposed at the end of Section 2.2.1 was applied to all systems, which in fact extends their original dimming ranges.

From Fig. 6(a), we can observe that the proposed MPPM-RPO-OFDM scheme using eU-OFDM or ACO-OFDM achieves a higher γ than RPO-OFDM or MPPM-OFDM does, provided that the

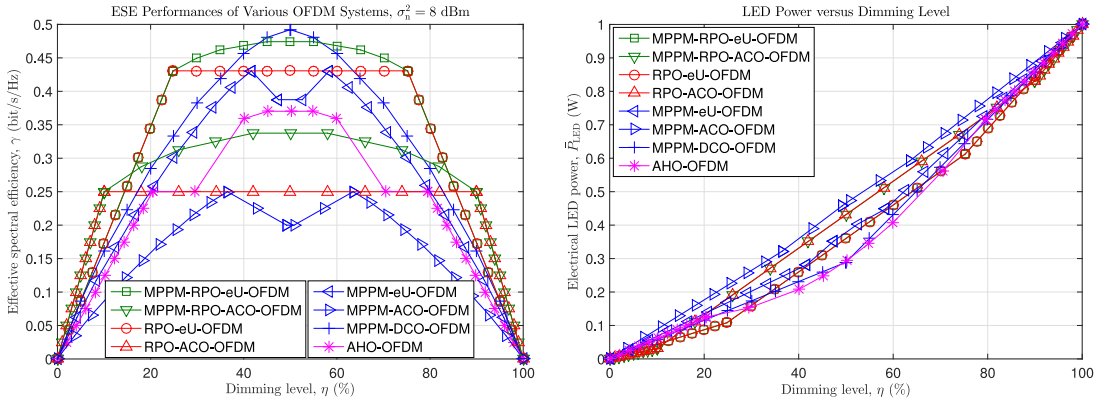

Fig. 6. The ESE and LED power versus η performances of various systems. (a) ESE, $\sigma_n^2 = 8$ dBm. (b) LED power.

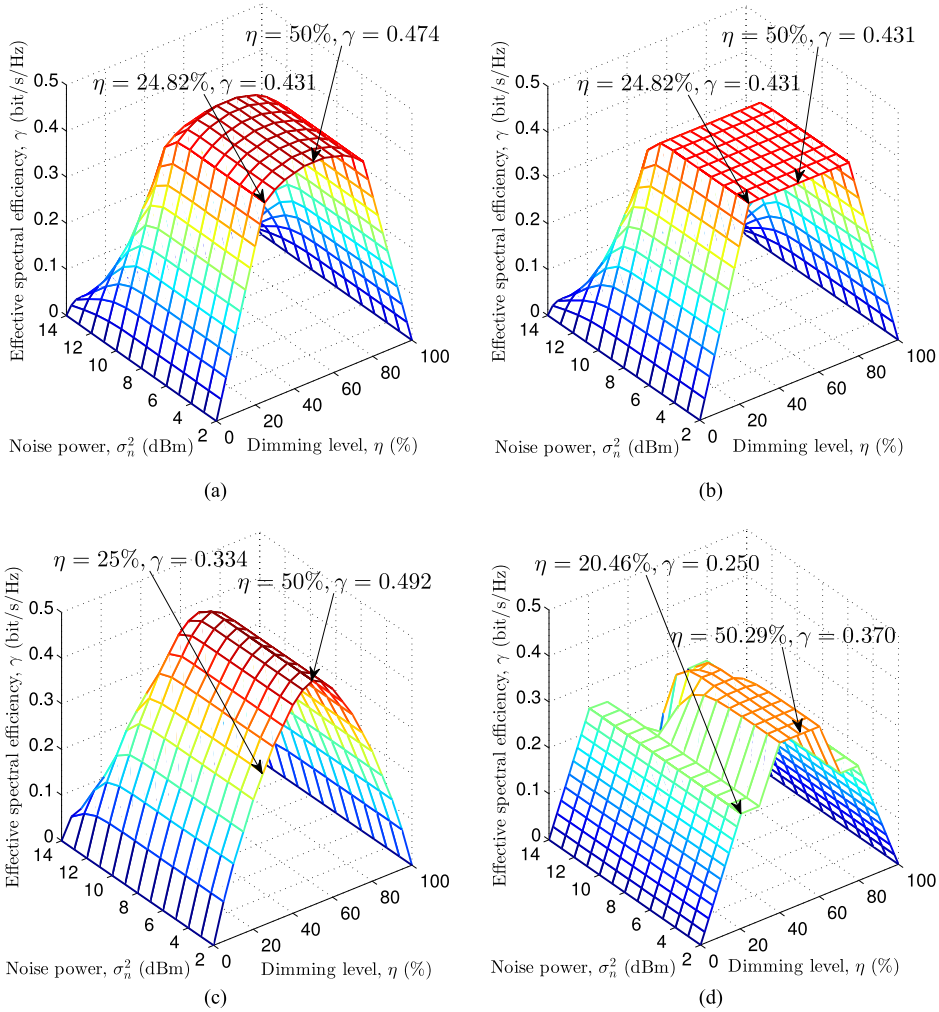

Fig. 7. The ESE performances of the systems as a function of σ_n^2 and η. (a) MPPM-RPO-eU-OFDM. (b) RPO-eU-OFDM. (c) MPPM-DCO-OFDM. (d) AHO-OFDM.

TABLE 3
Main Modules Required by Various Systems

Modules \ Scheme	MPPM-RPO-OFDM	RPO-OFDM	MPPM-OFDM	AHO-OFDM
TPI/RPI	√	√		
MPPM pattern selection	√		√	
MPPM demodulation	√		√	
Noise subtraction, additional FFT/IFFT/clipping				√

TABLE 4
The Comparison of Complexities of Various Systems

Scheme		Complexity	RAO/bit
MPPM-RPO-eU-OFDM	MUL	$p(6N\log_2 N+3N)$	996.1
	ADD	$p(9N\log_2 N)+lm(a-1)+\frac{pN}{2^D-1}[2^D(3D-1)+1]$	
	COM	$\frac{pN}{2^D-1}2^{D+2}+p(2N)+l[2\mathcal{B}_{\mathrm{MPPM}}+w\lceil\log_2(C_m^w)\rceil+\frac{(2m-w-1)w}{2}]$	
MPPM-RPO-ACO-OFDM	MUL	$p(3N\log_2 N+2N)$	1000.8
	ADD	$p(\frac{9}{2}N\log_2 N+2N)+lm(a-1)$	
	COM	$p(5N)+l[2\mathcal{B}_{\mathrm{MPPM}}+w\lceil\log_2(C_m^w)\rceil+\frac{(2m-w-1)w}{2}]$	
RPO-eU-OFDM	MUL	$p(6N\log_2 N+3N)$	994.4
	ADD	$p(9N\log_2 N)+\frac{pN}{2^D-1}[2^D(3D-1)+1]$	
	COM	$\frac{pN}{2^D-1}2^{D+2}+p(2N)$	
RPO-ACO-OFDM	MUL	$p(3N\log_2 N+2N)$	997.0
	ADD	$p(\frac{9}{2}N\log_2 N+2N)$	
	COM	$p(5N)$	
MPPM-eU-OFDM	MUL	$p(6N\log_2 N+3N)$	994.9
	ADD	$p(9N\log_2 N)+lm(a-1)+\frac{pN}{2^D-1}[2^D(3D-1)+1]$	
	COM	$\frac{pN}{2^D-1}2^D+p(2N)+2lma+l[2\mathcal{B}_{\mathrm{MPPM}}+w\lceil\log_2(C_m^w)\rceil+\frac{(2m-w-1)w}{2}]$	
MPPM-ACO-OFDM	MUL	$p(3N\log_2 N+2N)$	997.4
	ADD	$p(\frac{9}{2}N\log_2 N+2N)+lm(a-1)$	
	COM	$p(2N)+2lma+l[2\mathcal{B}_{\mathrm{MPPM}}+w\lceil\log_2(C_m^w)\rceil+\frac{(2m-w-1)w}{2}]$	
MPPM-DCO-OFDM	MUL	$p(4N\log_2 N+2N)$	660.2
	ADD	$p(6N\log_2 N+2N)+lm(a-1)$	
	COM	$p(2N)+2lma+l[2\mathcal{B}_{\mathrm{MPPM}}+w\lceil\log_2(C_m^w)\rceil+\frac{(2m-w-1)w}{2}]$	
AHO-OFDM	MUL	$p(7N\log_2 N+4N)$	1538.3
	ADD	$p(\frac{21}{2}N\log_2 N+\frac{13N}{4}-1)$	
	COM	$p(5N)$	

same optical OFDM scheme is employed. In addition, MPPM-RPO-eU-OFDM outperforms all other schemes in the majority of the practical dimming range, despite that its ESE performance is slightly lower than that of MPPM-DCO-OFDM when $\eta \in [45\%, 55\%]$. For a better demonstration, Fig. 7 shows the ESE results of the various systems in a three-dimensional way as a function of both η and σ_n^2. Both Figs. 6(a) and 7 prove that while also supporting a wide dimming range, the MPPM-RPO-eU-OFDM scheme can achieve the best ESE, or error-free SE, in most regions of η and σ_n^2, thanks to its capability of simultaneously accommodating more bits than existing methods.

Furthermore, the above-mentioned benefits are achievable without the need of an unproportionately high LED power, as revealed by Fig. 6(b), where we compare the values of $\bar{P}_{\mathrm{LED}}$ imposed by the various schemes. It shows that at the same dimming level η, $\bar{P}_{\mathrm{LED}}$ of the MPPM-RPO-eU-OFDM system is close to those of other reference systems.

4.3 Complexity Analysis

Table 3 outlines the main modules of the various systems studied with the common OFDM modulator and demodulator excluded, while Table 4 summarises their corresponding complexities, where $\lceil x \rceil$ indicates the minimum integer greater than or equal to x and D denotes the number of layers of eU-OFDM. Note that although we do not consider the complexity related to FEC for all schemes,

the DF-related complexity is counted for all MPPM variants. According to [22], an 80486 processor takes 13-42 clock cycles for one multiplication (MUL), and one cycle for one addition (ADD) or comparison (COM) operation. Thus, without loss of generality, we assume that the computational complexity of one real multiplication is equivalent to that of 20 real additions or comparisons. Then, we compute the equivalent complexities in terms of real addition operations (RAO) per bit for all systems with the parameters used in previous simulations, as seen in the right-most column of Table 4. Noting that the complexities of some schemes vary with different w, only the highest complexity values are provided. Table 4 implies that the demonstrated performance benefits of the proposed scheme are achievable with a modest computational complexity, which is at the same order as those of existing methods.

5. Conclusion

In this paper, we propose a hybrid MPPM-RPO-OFDM scheme to enhance the achievable SE for dimmable VLC systems. Through exploiting MPPM patterns for delivery of additional bits, the overall data rate can be improved by up to 35% within a wide dimming rage. Detailed theoretical performance analyses on the dimming level, the average electrical LED power consumption as well as the FEP of the proposed system are provided, which are verified by simulation results. We show that in comparison to many existing schemes such as MPPM-OFDM, RPO-OFDM and AHO-OFDM, the proposed scheme is capable of achieving the highest ESE in most of the scenarios, without substantially increasing the computational complexity or the LED power.

Appendix A
Derivation of $\bar{P}_{\mathrm{LED}}$

We assume that the bipolar time-domain OFDM signal samples before clipping are mutually independent and follow Gaussian distribution with zero mean [15]. Therefore, the probabilities that an ACO-OFDM sample is equal to zero and higher than $(I_{\mathrm{H}} - I_{\mathrm{L}})$ are $\frac{1}{2}$ and $Q\left(\frac{I_{\mathrm{H}}-I_{\mathrm{L}}}{\sigma}\right)$, respectively. Denote $s_{\mathrm{c,off}}$ and $s_{\mathrm{c,on}}$ as the sample values of the MPPM-RPO-OFDM signal $\mathbf{s}_{\mathrm{c}}$ at 'off' and 'on' slots, respectively.

Firstly, let us consider $s_{\mathrm{c,off}}$, which is generated by forcing the ACO-OFDM signal into the range of $[I_{\mathrm{L}}, I_{\mathrm{H}}]$, as indicated by (3) and (4). Thus, the probabilities that $s_{\mathrm{c,off}}$ is equal to I_{L} and I_{H} are $\frac{1}{2}$ and $Q\left(\frac{I_{\mathrm{H}}-I_{\mathrm{L}}}{\sigma}\right)$, respectively. Then the PDF of $s_{\mathrm{c,off}}$, denoted as $f_{s_{\mathrm{c,off}}}(x)$, can be calculated by

$$f_{s_{\mathrm{c,off}}}(x) = \begin{cases} \frac{1}{2}\delta(x - I_{\mathrm{L}}), & x \le I_{\mathrm{L}} \\ \frac{1}{\sigma}\phi\left(\frac{x-I_{\mathrm{L}}}{\sigma}\right), & I_{\mathrm{L}} < x < I_{\mathrm{H}} \\ Q\left(\frac{I_{\mathrm{H}}-I_{\mathrm{L}}}{\sigma}\right) \cdot \delta\left(x - I_{\mathrm{H}}\right), & x \ge I_{\mathrm{H}} \end{cases}, \tag{22}$$

where $\delta(\cdot)$ is Dirac delta function. According to the RPO property, we have $s_{\mathrm{c,on}} = I_{\mathrm{H}} + I_{\mathrm{L}} - s_{\mathrm{c,off}}$. The PDF of $s_{\mathrm{c,on}}$ can thus be given by

$$f_{s_{\mathrm{c,on}}}(x) = f_{s_{\mathrm{c,off}}}(I_{\mathrm{H}} + I_{\mathrm{L}} - x). \tag{23}$$

Therefore, $\bar{P}_{\mathrm{LED}}$ of MPPM-RPO-OFDM and RPO-OFDM systems can be obtained as

$$\bar{P}_{\mathrm{LED,MRO}} = \bar{P}_{\mathrm{LED,RO}} = \mathrm{E}(x^2) = \int_{-\infty}^{+\infty} x^2 \left[(1-d) \cdot f_{s_{\mathrm{c,off}}}(x) + d \cdot f_{s_{\mathrm{c,on}}}(x)\right] \mathrm{d}x, \tag{24}$$

which can be further developed into (12). On the other hand, $\bar{P}_{\mathrm{LED}}$ of MPPM-OFDM system can be formulated by

$$\bar{P}_{\mathrm{LED,MO}} = \mathrm{E}(x^2) = \int_{-\infty}^{+\infty} x^2 \cdot d \cdot f_{s_{\mathrm{c,off}}}(x) \mathrm{d}x, \tag{25}$$

which leads to (13).

Appendix B
Derivation of $\rho_{\mathrm{MPPM}}^{(\mathrm{c})}$

Since an MPPM symbol is constituted by 'off' and 'on' slots, the received signal $\bar{r}_{u,v}$ of (6) can therefore be decoupled with the aid of (5) into two component signals at 'off' and 'on' slots, denoted as $\bar{r}_{\mathrm{off}}$ and $\bar{r}_{\mathrm{on}}$, respectively

$$\begin{aligned}\bar{r}_{\mathrm{off}} &= \frac{1}{a}\sum_{k=1}^{a}\left(s_{\mathrm{c,off},k}+n_k\right) = \frac{1}{a}\sum_{k=1}^{a}s_{\mathrm{c,off},k}+\frac{1}{a}\sum_{k=1}^{a}n_k\\ \bar{r}_{\mathrm{on}} &= \frac{1}{a}\sum_{k=1}^{a}\left(s_{\mathrm{c,on},k}+n_k\right) = \frac{1}{a}\sum_{k=1}^{a}s_{\mathrm{c,on},k}+\frac{1}{a}\sum_{k=1}^{a}n_k,\end{aligned} \tag{26}$$

where $s_{\mathrm{c,off},k}$ and $s_{\mathrm{c,on},k}$ are the kth samples at 'off' and 'on' slots of $\mathbf{s}_{\mathrm{c}}$, respectively, while n_k is AWGN. Let $\bar{s}_{\mathrm{c,off}} = \frac{1}{a}\sum_{k=1}^{a}s_{\mathrm{c,off},k}$, $\bar{s}_{\mathrm{c,on}} = \frac{1}{a}\sum_{k=1}^{a}s_{\mathrm{c,on},k}$, and $\bar{n} = \frac{1}{a}\sum_{k=1}^{a}n_k$, then (26) can be rewritten as

$$\begin{aligned}\bar{r}_{\mathrm{off}} &= \bar{s}_{\mathrm{c,off}}+\bar{n}\\ \bar{r}_{\mathrm{on}} &= \bar{s}_{\mathrm{c,on}}+\bar{n}.\end{aligned} \tag{27}$$

If we denote the CFs of $s_{\mathrm{c,off},k}$ and $s_{\mathrm{c,on},k}$ as $\varphi_{s_{\mathrm{c,off}}}(\omega)$ and $\varphi_{s_{\mathrm{c,on}}}(\omega)$, respectively, then by exploiting [17, Theorem 3.3.1, Theorem 3.3.2], the CFs of $\bar{s}_{\mathrm{c,off}}$ and $\bar{s}_{\mathrm{c,on}}$ can be calculated by

$$\begin{aligned}\varphi_{\bar{s}_{\mathrm{c,off}}}(\omega) &= \left[\varphi_{s_{\mathrm{c,off}}}\left(\frac{\omega}{a}\right)\right]^a\\ \varphi_{\bar{s}_{\mathrm{c,on}}}(\omega) &= \left[\varphi_{s_{\mathrm{c,on}}}\left(\frac{\omega}{a}\right)\right]^a.\end{aligned} \tag{28}$$

With the aid of (23) and [17, Theorem 3.3.1], we arrive at $\varphi_{s_{\mathrm{c,on}}}(\omega) = \exp\left[\mathrm{j}\omega(I_{\mathrm{H}}+I_{\mathrm{L}})\right]\cdot\varphi_{s_{\mathrm{c,off}}}(-\omega)$. Since $\bar{n}$ in (27) follow zero-mean Gaussian distribution with variance $\frac{\sigma_{\mathrm{n}}^2}{a}$, according to [17, Example 3.3.3], the CF of $\bar{n}$ is

$$\varphi_{\bar{n}}(\omega) = \sqrt{2\pi}\phi\left(\frac{\sigma_{\mathrm{n}}\omega}{\sqrt{a}}\right). \tag{29}$$

One the other hand, let the PDFs of $\bar{r}_{\mathrm{off}}$ and $\bar{r}_{\mathrm{on}}$ be $f_{\bar{r}_{\mathrm{off}}}(x)$ and $f_{\bar{r}_{\mathrm{on}}}(x)$, respectively, and their CFs be $\varphi_{\bar{r}_{\mathrm{off}}}(\omega)$ and $\varphi_{\bar{r}_{\mathrm{on}}}(\omega)$, respectively. Exploiting (27)–(29) and [17, Theorem 3.3.2], we have

$$\varphi_{\bar{r}_{\mathrm{off}}}(\omega) = \varphi_{\bar{n}}(\omega)\varphi_{\bar{s}_{\mathrm{c,off}}}(\omega) = \sqrt{2\pi}\phi\left(\frac{\sigma_{\mathrm{n}}\omega}{\sqrt{a}}\right)\left[\varphi_{s_{\mathrm{c,off}}}\left(\frac{\omega}{a}\right)\right]^a \tag{30}$$

and

$$\begin{aligned}\varphi_{\bar{r}_{\mathrm{on}}}(\omega) &= \varphi_{\mathrm{n}}(\omega)\varphi_{\bar{s}_{\mathrm{c,on}}}(\omega)\\ &= \sqrt{2\pi}\phi\left(\frac{\sigma_{\mathrm{n}}\omega}{\sqrt{a}}\right)\left[\varphi_{s_{\mathrm{c,on}}}(x)\left(\frac{\omega}{a}\right)\right]^a = \sqrt{2\pi}\phi\left(\frac{\sigma_{\mathrm{n}}\omega}{\sqrt{a}}\right)\exp\left[\mathrm{j}\omega(I_{\mathrm{H}}+I_{\mathrm{L}})\right]\cdot\left[\varphi_{s_{\mathrm{c,off}}}\left(-\frac{\omega}{a}\right)\right]^a.\end{aligned} \tag{31}$$

Inserting (30) into (31), we have

$$\varphi_{\bar{r}_{\mathrm{on}}}(\omega) = \exp\left[\mathrm{j}\omega(I_{\mathrm{H}}+I_{\mathrm{L}})\right]\varphi_{\bar{r}_{\mathrm{off}}}(-\omega). \tag{32}$$

Based on (32) and using [17, Theorem 3.3.1], we can obtain

$$f_{\bar{r}_{\mathrm{on}}}(x) = f_{\bar{r}_{\mathrm{off}}}\left(I_{\mathrm{H}}+I_{\mathrm{L}}-x\right). \tag{33}$$

As discussed in Section 2.1.2, when demodulating the uth MPPM symbol, a total of w slots having the largest w values of $\bar{r}_{u,v}$ defined by (6), are considered as the 'on' slots, while the other $(m-w)$ slots are assumed to be the 'off' slots. Based on such a demodulation principle, it implies that an MPPM symbol would be correctly demodulated, iff $\bar{r}_{\mathrm{on}}$ of all the 'on' slots of this specific MPPM symbol are larger than $\bar{r}_{\mathrm{off}}$ of all the 'off' slots. This necessary and sufficient condition can

be described by

$$\bar{r}_{\text{on,min}} = \min_{1\le k\le w}\left\{\bar{r}_{\text{on},k}\right\} > \bar{r}_{\text{off,max}} = \max_{1\le k\le (m-w)}\left\{\bar{r}_{\text{off},k}\right\}, \tag{34}$$

where $\bar{r}_{\text{on},k}$ and $\bar{r}_{\text{off},k}$ refer to $\bar{r}_{\text{on}}$ at the kth 'on' slot and $\bar{r}_{\text{off}}$ at the kth 'off' slot, respectively.

Let $F_{\bar{r}_{\text{off,max}}}(x)$ and $f_{\bar{r}_{\text{off,max}}}(x)$ denote the cumulative distribution function (CDF) and the PDF of $\bar{r}_{\text{off,max}}$, respectively. Similarly, define $F_{\bar{r}_{\text{on,min}}}(x)$ and $f_{\bar{r}_{\text{on,min}}}(x)$ as the CDF and PDF of $\bar{r}_{\text{on,min}}$, respectively. Then we have

$$\begin{aligned} F_{\bar{r}_{\text{off,max}}}(x) &= \rho\left(\bar{r}_{\text{off,max}} \le x\right) = \rho\left(\bar{r}_{\text{off},1} \le x, \ldots, \bar{r}_{\text{off},m-w} \le x\right) = \left[\int_{-\infty}^{x} f_{\bar{r}_{\text{off}}}(t)\mathrm{d}t\right]^{m-w} \\ f_{\bar{r}_{\text{off,max}}}(x) &= \frac{\mathrm{d}F_{\bar{r}_{\text{off,max}}}}{\mathrm{d}x} = (m-w)\cdot f_{\bar{r}_{\text{off}}}(x)\cdot\left[\int_{-\infty}^{x} f_{\bar{r}_{\text{off}}}(t)\mathrm{d}t\right]^{m-w-1} \end{aligned} \tag{35}$$

and

$$\begin{aligned} F_{\bar{r}_{\text{on,min}}}(x) &= \rho\left(\bar{r}_{\text{on,min}} \le x\right) = 1-\rho\left(\bar{r}_{\text{on,min}} > x\right) = 1-\rho\left(\bar{r}_{\text{on},1} > x, \ldots, \bar{r}_{\text{on},w} > x\right) \\ &= 1-\left[1-\int_{-\infty}^{x} f_{\bar{r}_{\text{on}}}(t)\mathrm{d}t\right]^{w} \\ f_{\bar{r}_{\text{on,min}}}(x) &= \frac{\mathrm{d}F_{\bar{r}_{\text{on,min}}}}{\mathrm{d}x} = w\cdot f_{\bar{r}_{\text{on}}}(x)\cdot\left[1-\int_{-\infty}^{x} f_{\bar{r}_{\text{on}}}(t)\mathrm{d}t\right]^{w-1}, \end{aligned} \tag{36}$$

where $\rho(\cdot)$ denotes the probability function.

Since $\rho^{(\text{c})}_{\text{MPPM}}$ equals the probability of the condition specified in (34), we can therefore calculate it by utilising (33), (35), and (36), yielding

$$\begin{aligned} \rho^{(\text{c})}_{\text{MPPM}} &= \int_{-\infty}^{+\infty}\int_{-\infty}^{x} f_{\bar{r}_{\text{on,min}}}(x) f_{\bar{r}_{\text{off,max}}}(t)\mathrm{d}t\mathrm{d}x \\ &= \int_{-\infty}^{+\infty} f_{\bar{r}_{\text{on,min}}}(x) F_{\bar{r}_{\text{off,max}}}(x)\mathrm{d}x \\ &= \int_{-\infty}^{+\infty} w f_{\bar{r}_{\text{on}}}(x)\left[1-\int_{-\infty}^{x} f_{\bar{r}_{\text{on}}}(t)\mathrm{d}t\right]^{w-1} F_{\bar{r}_{\text{off,max}}}(x)\mathrm{d}x \\ &= \int_{-\infty}^{+\infty} w f_{\bar{r}_{\text{off}}}(I_{\text{H}}+I_{\text{L}}-x)\cdot\left[\int_{-\infty}^{I_{\text{H}}+I_{\text{L}}-x} f_{\bar{r}_{\text{off}}}(t)\mathrm{d}t\right]^{w-1} F_{\bar{r}_{\text{off,max}}}(x)\mathrm{d}x \\ &= \int_{-\infty}^{+\infty} w f_{\bar{r}_{\text{off}}}(x)\left[\int_{-\infty}^{x} f_{\bar{r}_{\text{off}}}(t)\mathrm{d}t\right]^{w-1}\cdot F_{\bar{r}_{\text{off,max}}}(I_{\text{H}}+I_{\text{L}}-x)\,\mathrm{d}x \\ &= w\int_{-\infty}^{+\infty} f_{\bar{r}_{\text{off}}}(x)\left[\int_{-\infty}^{x} f_{\bar{r}_{\text{off}}}(t)\mathrm{d}t\right]^{w-1}\cdot\left[\int_{-\infty}^{I_{\text{H}}+I_{\text{L}}-x} f_{\bar{r}_{\text{off}}}(t)\mathrm{d}t\right]^{m-w}\mathrm{d}x, \end{aligned} \tag{37}$$

which arrives at (18), where [17, Theorem 3.3.5]

$$f_{\bar{r}_{\text{off}}}(x) = \frac{1}{2\pi}\int_{-\infty}^{+\infty}\varphi_{\bar{r}_{\text{off}}}(\omega)\exp\left(-\mathrm{j}\omega x\right)\mathrm{d}\omega. \tag{38}$$

Finally, we can obtain (19) by substituting (30) into (38).

Appendix C
Approximation of (18)

As mentioned at the end of Section 2.2.3, it is necessary to simplify (18) for computation aspect. More specifically, we replace $-\infty$ with λ_1 and $+\infty$ with λ_2 in (18), where $\lambda_i\,(i=1,2)$ are

approximation parameters, yielding

$$\rho_{\mathrm{MPPM}}^{(\mathrm{c})} = w\left\{\int_{\lambda_1}^{\lambda_2} f_{\bar{r}_{\mathrm{off}}}(x)\left[\int_{\lambda_1}^{x} f_{\bar{r}_{\mathrm{off}}}(t)\mathrm{d}t + \varepsilon_1\right]^{w-1}\cdot\left[\int_{\lambda_1}^{l_{\mathrm{H}}+l_{\mathrm{L}}-x} f_{\bar{r}_{\mathrm{off}}}(t)\mathrm{d}t + \varepsilon_2\right]^{m-w}\mathrm{d}x + \varepsilon_3\right\}, \tag{39}$$

where, since $\int_{-\infty}^{+\infty} f_{\bar{r}_{\mathrm{off}}}(t)\mathrm{d}t = 1$ and $f_{\bar{r}_{\mathrm{off}}}(t) \geq 0$, we have

$$\varepsilon_1 = \varepsilon_2 = \int_{-\infty}^{\lambda_1} f_{\bar{r}_{\mathrm{off}}}(t)\mathrm{d}t \leq 1 - \int_{\lambda_1}^{\lambda_2} f_{\bar{r}_{\mathrm{off}}}(t)\mathrm{d}t, \tag{40}$$

while

$$\begin{aligned}\varepsilon_3 = &\int_{-\infty}^{\lambda_1} f_{\bar{r}_{\mathrm{off}}}(x)\left[\int_{-\infty}^{x} f_{\bar{r}_{\mathrm{off}}}(t)\mathrm{d}t\right]^{w-1}\cdot\left[\int_{-\infty}^{l_{\mathrm{H}}+l_{\mathrm{L}}-x} f_{\bar{r}_{\mathrm{off}}}(t)\mathrm{d}t\right]^{m-w}\mathrm{d}x\\ &+\int_{\lambda_2}^{+\infty} f_{\bar{r}_{\mathrm{off}}}(x)\left[\int_{-\infty}^{x} f_{\bar{r}_{\mathrm{off}}}(t)\mathrm{d}t\right]^{w-1}\cdot\left[\int_{-\infty}^{l_{\mathrm{H}}+l_{\mathrm{L}}-x} f_{\bar{r}_{\mathrm{off}}}(t)\mathrm{d}t\right]^{m-w}\mathrm{d}x.\end{aligned} \tag{41}$$

Noting that

$$0 \leq \left[\int_{-\infty}^{x} f_{\bar{r}_{\mathrm{off}}}(t)\mathrm{d}t\right]^{w-1}\cdot\left[\int_{-\infty}^{l_{\mathrm{H}}+l_{\mathrm{L}}-x} f_{\bar{r}_{\mathrm{off}}}(t)\mathrm{d}t\right]^{m-w} \leq 1 \tag{42}$$

for all $x \in \mathbb{R}$, we can therefore simplify ε_3 of (41) to

$$\varepsilon_3 \leq \int_{-\infty}^{\lambda_1} f_{\bar{r}_{\mathrm{off}}}(x)\mathrm{d}x + \int_{\lambda_2}^{+\infty} f_{\bar{r}_{\mathrm{off}}}(x)\mathrm{d}x = 1 - \int_{\lambda_1}^{\lambda_2} f_{\bar{r}_{\mathrm{off}}}(x)\mathrm{d}x. \tag{43}$$

Hence, with the aid of (40) and (43) and the given system parameters, $\lambda_i\,(i = 1, 2)$ in (39) can be appropriately selected to strike for a tradeoff between model accuracy and computation efficiency. Considering the simulation parameters stated in Section 4, the values of $\lambda_1 = -1$ and $\lambda_2 = 2$ can be selected to ensure the upper-bounded ε_1, ε_2 and ε_3 do not exceed a predefined small threshold, for example 10^{-6}. Then, (39) can be approximated as

$$\rho_{\mathrm{MPPM}}^{(\mathrm{c})} \approx w\left\{\int_{\lambda_1}^{\lambda_2} f_{\bar{r}_{\mathrm{off}}}(x)\left[\int_{\lambda_1}^{x} f_{\bar{r}_{\mathrm{off}}}(t)\mathrm{d}t\right]^{w-1}\cdot\left[\int_{\lambda_1}^{l_{\mathrm{H}}+l_{\mathrm{L}}-x} f_{\bar{r}_{\mathrm{off}}}(t)\mathrm{d}t\right]^{m-w}\mathrm{d}x\right\} \tag{44}$$

by setting $\varepsilon_i = 0\,(i = 1, 2, 3)$. Based on the aforementioned parameters and (44), the theoretical curves in Fig. 4(a) and (b) can be generated.

Acknowledgment

The authors would like to thank H. Huang, F. Fang, W. Chen, and Z. Liu for their kind support to the experiment work of this paper.

References

[1] T. Komine and M. Nakagawa, "Fundamental analysis for visible-light communication system using LED lights," *IEEE Trans. Consum. Electron.*, vol. 50, no. 1, pp. 100–107, Feb. 2004.
[2] J. Gancarz, H. Elgala, and T. D. C. Little, "Impact of lighting requirements on VLC systems," *IEEE Commun. Mag.*, vol. 51, no. 12, pp. 34–41, Dec. 2013.
[3] S. C. J. Lee, S. Randel, F. Breyer, and A. M. J. Koonen, "PAM-DMT for intensity-modulated and direct-detection optical communication systems," *IEEE Photon. Technol. Lett.*, vol. 21, no. 23, pp. 1749–1751, Dec. 2009.
[4] J. Armstrong and A. J. Lowery, "Power efficient optical OFDM," *Electron. Lett.*, vol. 42, no. 6, pp. 370–372, Mar. 2006.
[5] J. Armstrong and B. J. C. Schmidt, "Comparison of asymmetrically clipped optical OFDM and DC-biased optical OFDM in AWGN," *IEEE Commun. Lett.*, vol. 12, no. 5, pp. 343–345, May 2008.
[6] S. D. Dissanayake and J. Armstrong, "Comparison of ACO-OFDM, DCO-OFDM and ADO-OFDM in IM/DD systems," *J. Lightw. Technol.*, vol. 31, no. 7, pp. 1063–1072, Apr. 2013.
[7] D. Tsonev, S. Sinanovic, and H. Haas, "Novel unipolar orthogonal frequency division multiplexing (U-OFDM) for optical wireless," in *Proc. 2012 IEEE 75th Veh. Technol. Conf.*, Yokohama, Japan, May 6–9, 2012, pp. 1–5.

[8] H. Elgala and T. D. C. Little, "P-OFDM: Spectrally efficient unipolar OFDM," in *Proc. Opt. Fiber Commun. Conf. Exhib.*, Washington, DC, USA, Mar. 9–13, 2014, Paper Th3G.7.
[9] D. Tsonev and H. Haas, "Avoiding spectral efficiency loss in unipolar OFDM for optical wireless communication," in *Proc. 2014 IEEE Int. Conf. Commun.*, Sydney, NSW, Australia, Jun. 10–14, 2014, pp. 3336–3341.
[10] Z. Wang, W.-D. Zhong, C. Yu, J. Chen, C. P. S. Francois, and W. Chen, "Performance of dimming control scheme in visible light communication system," *Opt. Exp.*, vol. 20, no. 17, pp. 18 861–18 868, Aug. 2012.
[11] X. You, J. Chen, H. Zheng, and C. Yu, "Efficient data transmission using MPPM dimming control in indoor visible light communication," *IEEE Photon. J.*, vol. 7, no. 4, Aug. 2015, Art. no. 7902512.
[12] H. Elgala and T. D. C. Little, "Reverse polarity optical-OFDM (RPO-OFDM): Dimming compatible OFDM for gigabit VLC links," *Opt. Exp.*, vol. 21, no. 20, pp. 24288–24299, Oct. 2013.
[13] Q. Wang, Z. Wang, and L. Dai, "Asymmetrical hybrid optical OFDM for visible light communications with dimming control," *IEEE Photon. Technol. Lett.*, vol. 27, no. 9, pp. 974–977, May 2015.
[14] S. Dimitrov, S. Sinanovic, and H. Haas, "Double-sided signal clipping in ACO-OFDM wireless communication system," in *Proc. 2011 IEEE Int. Conf. Commun.*, Kyoto, Japan, Jun. 5–9, 2011, pp. 1–5.
[15] S. H. Han and J. H. Lee, "An overview of peak-to-average power ratio reduction techniques for multicarrier transmission," *IEEE Wireless Commun.*, vol. 12, no. 2, pp. 56–65, Apr. 2005.
[16] M. K. Simon and M.-S. Alouini, *Digital Communication Over Fading Channels*, 2nd ed. Hoboken, NJ, USA: Wiley, 2005.
[17] R. Durrett, *Probability: Theory and Examples*, 4th ed., New York, NY, USA: Cambridge Univ. Press, 2010.
[18] A. Halder and A. D. Barman, "Nonlinear compensation of LEDs for improved performance in CSK based indoor visible light communication," in *Proc. 2015 6th Int. Conf. Comput. Devices Commun.*, Kolkata, India, Dec. 16–18, 2015, pp. 1–4.
[19] A. Halder and A. D. Barman, "Adaptive pre-compensation of LEDs for improved decoding of N-CSK in visible light communication," in *Proc. 2016 Int.Conf. Numer. Simulation Optoelectro. Devices*, Sydney, NSW, Australia, Jul. 11–15, 2016, pp. 143–144.
[20] D. Tsonev, S. Sinanovic, and H. Haas, "Complete modeling of nonlinear distortion in OFDM-based optical wireless communication," *J. Lightw. Technol.*, vol. 31, no. 18, pp. 3064–3076, Sep. 2013.
[21] K. Cai and M. Jiang, "SM/SPPM aided multiuser precoded visible light communication systems," *IEEE Photon. J.*, vol. 8, no. 2, Apr. 2016, Art. no. 7902109.
[22] M. A. Mazidi and J. G. Mazidi, *The 80 × 86 IBM PC and Compatible Computers (Volumes I & II)*, 4th ed. Upper Saddle River, NJ, USA: Pearson Education, 2003.